Nuclear Physics **A365** (1981) 349–370

MOMENTUM DISTRIBUTION OF NUCLEONS IN THE DEUTERON FROM THE d(e, e'p)n REACTION

M. BERNHEIM, A. BUSSIÈRE, J. MOUGEY*, D. ROYER, D. TARNOWSKI and S. TURCK-CHIEZE

DPh-N/HE, CEN Saclay, 91191 Gif-sur-Yvette Cedex, France

S. FRULLANI

Laboratorio delle Radiazioni, Istituto Superiore di Sanità, Sezione Sanità, Istituto Nazionale di Fisica Nucleare, Roma, Italy

G.P. CAPITANI and E. DE SANCTIS

Laboratori Nazionali di Frascati, INFN, 00044 Frascati (Roma) Italy

and

E. JANS**

National Institute for Nuclear and High Energy Physics (Formerly IKO), Amsterdam, The Netherlands

Received 12 January 1981

Abstract: The nucleon momentum distribution in the deuteron has been determined up to 340 MeV/c by measuring the d(e, e'p)n reaction at an incident electron energy of 500 MeV. The data are well described even above $p = 200$ MeV/c by the most recent deuteron wave functions, in contrast with previous (e, e'p) and (p, 2p) results.

E | NUCLEAR REACTION ^{2}H(e, e'p), $E = 500$ MeV; measured σ, missing energy, recoil momentum. ^{2}H deduced effective nucleon momentum distribution. Liquid target.

1. Introduction

The electrodisintegration of the deuteron has been proved to be an essential tool to study the structure of the two-nucleon system [1]. Deuterium has been used as a neutron target to get information on the neutron electromagnetic form factors, both in single arm, (e, e') [ref. [2])], or in coincidence, (e, e'p) and (e, e'n) experiments [ref. [3])]. Recent measurements at threshold, far from the quasi-elastic region [4], have provided some of the clearest evidence for meson exchange currents in the spin–flip transition to the unbound singlet state near threshold.

Coincidence (e, e'p) experiments, under conditions of quasi-free e-p kinematics provide the most direct way of measuring the nucleon momentum distribution inside the deuteron [5]. Within the one-photon-exchange impulse approximation (fig. 1), the

* Present address: Institut Laue-Langevin, F-38042 Grenoble Cedex.

** Supported by Dutch Foundation for Fundamental Research on Matter (FOM).

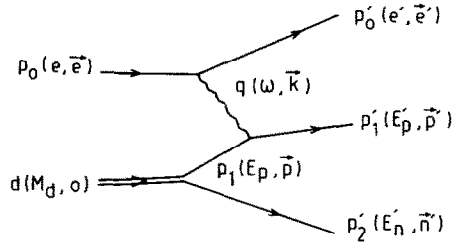

Fig. 1. The quasi-free d(e, e'p)n process. We indicate our notation for the energy-momentum four vector in the laboratory system for each particle line. p_0, p'_0 represent the incoming and scattered electrons, p'_1, p'_2 the outgoing proton and neutron, d the initial deuteron, and p_1 the "initial proton" inside the deuteron.

d(e, e'p)n reaction is described as follows: an energy $\omega = e - e'$ and a momentum $\boldsymbol{k} = \boldsymbol{e} - \boldsymbol{e}'$ are transferred from an incident electron to a target proton of initial momentum $\boldsymbol{p}$, which is ejected with a final momentum $\boldsymbol{p}'$, (total energy E'_p). The residual neutron simply recoils with a momentum $\boldsymbol{n}'$ (total energy E'_n). In such an approximation one has $\boldsymbol{p} = -\boldsymbol{n}' = \boldsymbol{p}' - \boldsymbol{k}$ and the cross section is simply written:

$$\frac{d\sigma}{de'\, dE'_p\, d\Omega_{e'}\, d\Omega_{p'}} = K \frac{d\sigma^{(p)}}{d\Omega_{e'}} \rho(p) \delta(E + E_B) , \tag{1}$$

where $d\sigma^{(p)}/d\Omega_{e'}$ is essentially the free e-p cross section, K a kinematical factor, and $\rho(p)$ represents the distribution of the proton momentum $\boldsymbol{p}$ inside the deuteron. The "missing energy" E is defined as $E = \omega - E'_p - E'_n + M_p + M_n$, M_p and M_n being the proton and neutron mass, respectively. The cross section is peaked at $E = -E_B = 2.23$ MeV, corresponding to the binding energy of the deuteron.

In a non-relativistic description, the momentum distribution ρ is written:

$$\rho(p) = \left| \int u(r) j_0(pr) r \, dr \right|^2 + \left| \int \omega(r) j_2(pr) r \, dr \right|^2 , \tag{2}$$

$u(r)$ and $\omega(r)$ being the radial wave functions for the S- and D-states, respectively [1,6].

Of particular interest is the D-state contribution, which is expected to dominate in the cross section for high p-values, as it gives direct insight into the tensor part of the nucleon–nucleon force. Similar information is contained in the electromagnetic structure functions $A(q^2)$ and $B(q^2)$ which one gets from elastic e-d scattering experiments, but their dependence upon $u(r)$ and $\omega(r)$, through the charge, quadrupole and magnetic form factors is much more complicated [6]. Moreover, it appears that the sensitivity to short-range aspects of the deuteron wave function is quite different in $A(q^2)$ and in $\rho(p)$ [ref. [7])]. Fig. 2 shows the two functions calculated with the Reid soft core potential. One sees that the dip in the S-state contribution, which appears at $q \sim 930$ MeV/c in the A distribution moves to ~ 400 MeV/$c \sim \frac{1}{2}q$ in the momentum distribution. A measurement of the (e, e'p) cross section in the region 300–500 MeV/c would give directly the corresponding Fourier components of the D-state amplitude. Together with other information available about the D-state

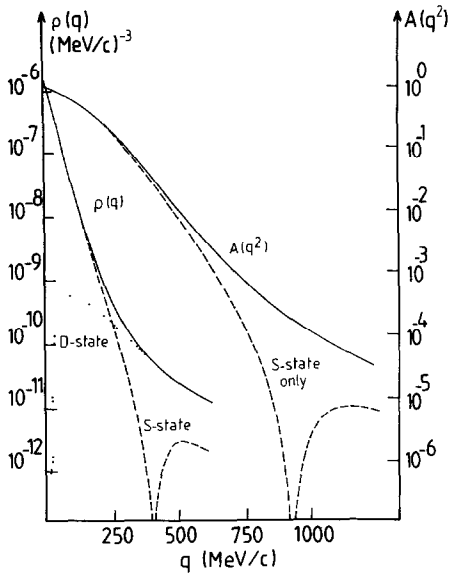

Fig. 2. The deuteron momentum density, $\rho(q)$, compared to the structure function, $A(q^2)$, both calculated from the Reid soft core potential. In our notations q in $\rho(q)$ is the initial proton momentum $\boldsymbol{p}$, whereas in $A(q^2)$ it is the four-momentum transfer. One sees that the momentum density falls much more rapidly with q than the structure function, and that the dip in the S-state contribution appears at lower momentum. Around $q = 400$ MeV/c, the density ρ is due to the deuteron D-state alone.

[deuteron quadrupole moment [8]), asymptotic normalisation [9])] such a measurement would put an important constraint on the nucleon–nucleon potential.

The first coincidence d(e, e'p)n experiments were performed in Stanford by Croissiaux [10]) with an incident energy $e = 500$ MeV and around $p = 0$, and in Orsay by Bounin [11]) for $e = 350$ MeV, up to $p = 94$ MeV/c. Measurements at $e = 1190$ MeV have been made in Kharkov by Antoufiev *et al.* [12]) up to $p = 185$ MeV/c. New data from Kharkov have been reported recently [13]), reaching $p \sim 300$ MeV/c. The limitation to rather low values of p in these experiments – except for the last one – was due to the rather poor duty cycle of the electron accelerators used together with the rapid variation of the cross section with p.

The major goal of the present experiment was to take advantage of the high-energy, high-duty cycle Saclay Linear Accelerator to extend the previous measurements up to the region where the D-state contribution dominates. The experimental method and apparatus will be described in sect. 2, and the measured cross sections, with a discussion of uncertainties, given in sect. 3. Certain effects usually neglected in the analysis of such experiments, such as the interference with e-n scattering, final state n-p interactions, and contributions from mesonic currents, will be briefly discussed in sect. 4. In sect. 5, we compare our results, in terms of a momentum distribution, to other (e, e'p) and (p, 2p) results (although the latter reaction really

involves three hadrons instead of two, thereby leading to more complex reaction mechanisms). We also show that our experimental data are in good overall agreement with recent theoretical predictions of the deuteron wave function.

2. Description of the experiment

The experiment was performed at the 600 MeV Linear Electron Accelerator of Saclay using the two-spectrometer arrangement of the HE1 experimental room. This experimental facility has already been described in detail [14]), so only its main characteristics are recalled here in table 1. It permits coincidence measurements in nearly coplanar kinematics, as sketched in fig. 3.

The detection system behind each spectrometer consists of two multiwire proportional chambers (MWPC) used as position detectors, together with plastic scintillators and Čerenkov counters used for fast triggering. The information from the MWPC are processed on line by a PDP 15/30 computer to give the energy and the vertical angle of trajectories for both the electron and the proton at the target point.

The beam intensity is monitored both by a Faraday cup, located in an adjacent room downstream from the beam, and a ferrite mounted just in front of the scattering chamber. For a 1 to 10 μA beam intensity, which was typical for this experiment, the two monitors agreed to within 1%.

2.1. THE LIQUID TARGET

The two-stage liquid D_2 target [15]) developed for this experiment is sketched in fig. 4. The liquid deuterium in the target is cooled 3°K below its normal boiling temperature by heat exchange with liquid hydrogen. Natural convection in the deuterium loop is produced by beam heating. The target is a 15 mm diameter vertical stainless steel cylinder, of wall thickness 0.02 mm. When the beam is focussed on the target (1×2 mm spot size) the effective deuterium thickness was found to decrease linearly with the beam intensity, with a slope of −2% per μA up to 9 μA; the slope was −0.5% per μA up to 25 μA when the beam was defocused (2×4 mm).

2.2. KINEMATICAL CONDITIONS

Of the nine kinematical variables necessary to completely describe the final state in the deuteron electrodisintegration process, five must be measured since four variables are determined by momentum and energy conservation. As described above, the detector arrangement allows the measurement of the electron and proton momentum magnitudes and vertical scattering angles. Together with the two horizontal angles of the spectrometers, the kinematics is overdetermined.

Two sets of data were taken, in which the transferred momentum, $|\boldsymbol{k}|$, and energy, ω, were kept constant. By working at a fixed momentum transfer, one keeps roughly

TABLE 1

Essential features of the ALS electron scattering facility

Spectrometers characteristics	"600"		"900"	
radius (c.m.)	140		180	
bending angle	153°		169°42′	
maximum rigidity (MeV/c)	630		900	
maximum solid angle (msr)	6.7		4.9	
horizontal aperture (mr)	34		35	
vertical aperture (mr)	200		140	
momentum acceptance	+10%, −30%		±5%	
momentum resolution	4×10^{-4}		1.5×10^{-4}	
Wire chambers characteristics	**E**	**X**	**E**	**X**
number of wires (2mm spacing)	1024	1152	512	640
number of detection channels	512	192	512	160
momentum of acceptance of a single channel (E chamber)	(6×10^{-4})		(2×10^{-4})	

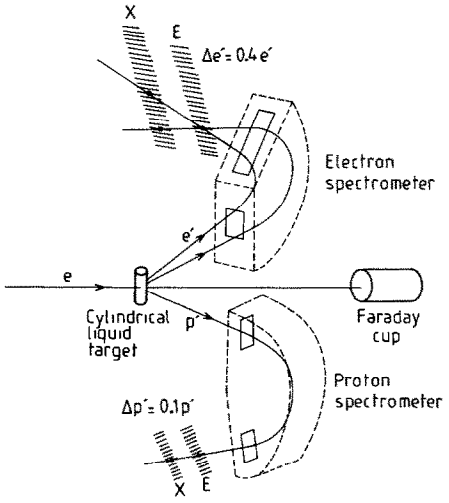

Fig. 3. Sketch of the experimental apparatus. The two vertical spectrometers permit one to vary the scattering angles in a coplanar kinematics. The use of two sets of multiwire chambers behind each spectrometer (indicated as E and X chamber on the figure) permits the reconstruction of the particle trajectories.

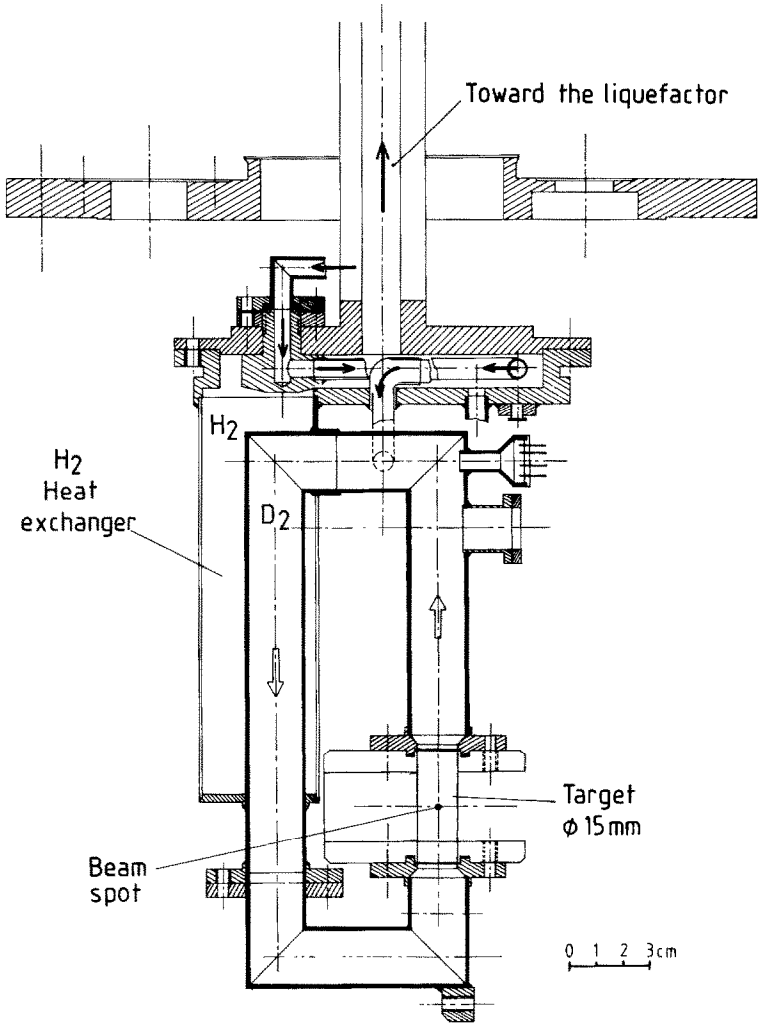

Fig. 4. Sketch of the two stage deuterium target. When heated by the beam, the deuterium starts to circulate by convection, and is cooled below its boiling point in passing through the liquid hydrogen heat exchanger.

constant the electron–proton scattering amplitude. Moreover, fixing both k and ω leads to a fixed value of the n-p relative energy $E_{np}^{c.m.}$ in the final state, which is given by

$$E_{np}^{c.m.} = [(\omega + M_d)^2 - \boldsymbol{k}^2]^{1/2} - (M_p + M_n)\,, \tag{3}$$

M_d being the deuteron mass. Keeping $E_{np}^{c.m.}$ constant makes the calculation of rescattering effects in the final state easier. The recoil momentum $\boldsymbol{n}'$ is varied by simultaneous changes of the analysed proton energy and angle.

TABLE 2

Kinematics conditions for the d(e, e'p)n experiment at 500 MeV

e' (MeV)	θ_e	k (MeV/c)	ω (MeV)	$E_{np}^{c.m.}$ (MeV)	$p^{c.m.}$ (MeV/c)	p' (MeV/c)	θ_p
Set I 395	59°	450	105	51.0	221	450.0	48.9°
						417.8	69.7°
Set II 352	44.4°	350	147	114.3	331	510.0	45.2°
						421.2	93.1°

For each of the two sets of kinematic conditions, only the extreme proton angle and corresponding momentum values are given. The outgoing electron and proton momenta correspond to the central values of the accepted ranges.

The two sets of kinematical parameters are given in table 2. For the first one, ω and $\boldsymbol{k}^2$ are related by $\omega = [\boldsymbol{k}^2 + M_p^2]^{1/2} - M_p$ allowing $\boldsymbol{n}' = 0$ when the proton is detected in the direction of $\boldsymbol{k}$. One sees on fig. 5 that, under kinematics I, the neutron recoils in a direction perpendicular to the outgoing proton. In the kinematics II, a lower value of 350 MeV/c has been chosen for k to increase the electron proton cross section and so to compensate for the decrease of the momentum distribution at high momenta.

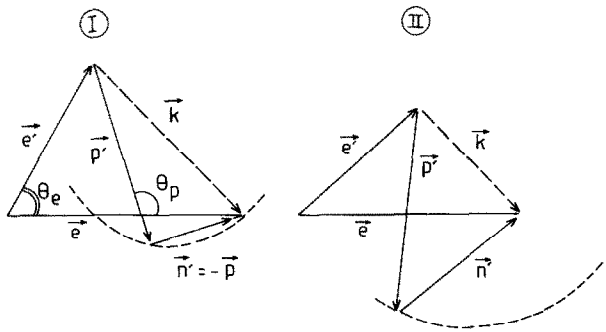

Fig. 5. Kinematics I (low p) and II (high p). For both kinematics, the electron parameters are fixed. One sees that the value $p = 0$ is allowed only in the kinematics I.

2.3. DATA ANALYSIS

A coincidence event is identified when one particle is detected in each spectrometer within a time interval of about 40 ns. This large coincidence window is necessary to account for the differences in time of flight due to the different energies and angles of the analysed particles. Using the information from the multiwire chambers, the trajectories are reconstructed and are required to have their origins inside the target volume. A time of flight correction is computed from the trajectory lengths, and a corrected time spectrum is established such as is shown on fig. 6. The

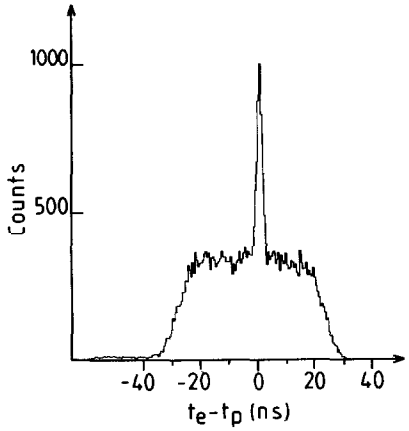

Fig. 6. Time difference spectrum between electrons and protons in the d(e, e'p)n experiment. The true coincidence events appear as a sharp peak (FWHM = 2.1 ns).

peak of true coincidences, with ~2 ns FWHM, appears on a flat background of accidental coincidences. The number of accidentals under the peak is estimated from the wings of the spectrum. The signal-to-noise ratio varied from 16 to 0.04 depending on the particular kinematics used and on the actual duty cycle of the beam. However, this ratio is about ten times larger if one considers only the events corresponding to a missing energy value inside a 10 MeV bin centered on the separation energy of the deuteron.

The next step is to compute the acceptance volumes and the distribution of accidental events in the region of the (p, E) plane, in which the cross section is to be extracted. This is done by a Monte Carlo calculation. The input data for the acceptance calculations are the momentum and angle limits of the spectrometers. A random generation of the reaction point within the effective target volume is combined with the solid angles of the spectrometers, known off the beam axis from previous measurements. The same calculation is made for the accidentals, with the measured energy spectra of electrons and protons as additional constraints. Fig. 7 shows the energy distributions for coincidences, calculated accidentals, and acceptance volumes. The mean value of the cross section after removing the accidentals should be zero for values of the missing energy which are below threshold or large enough to neglect the radiative tail of the reaction peak.

2.4. RADIATIVE CORRECTIONS

As for any electron scattering reaction, the one-photon exchange (e, e'p) process is accompanied by bremsstrahlung emission from the electron waves. This causes an additional energy loss, thus a reduction of the cross section at the break up energy. Standard formulas [16]) were used to compute these corrections, which appear as a

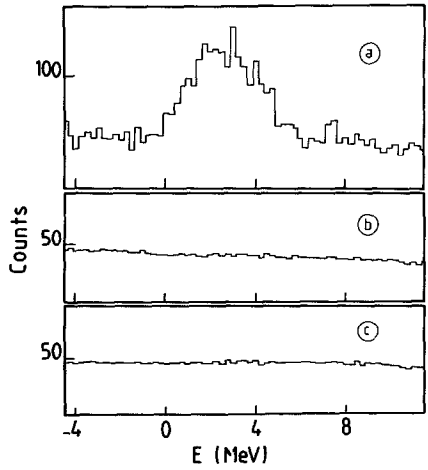

Fig. 7. Energy distributions for coincidences (a), calculated accidentals (b) and acceptance volumes (c), for the d(e, e'p)n reaction under the kinematical conditions: $e = 500$ MeV, $e' = 395$ MeV, $\theta_e = 44.4°$ $\theta_p = 74.4°$.

multiplicative factor to the sixfold differential experimental cross section integrated over the missing energy E up to $E = -E_B + \Delta E$ beyond the peak energy $-E_B$. Both the Schwinger term (bremsstrahlung emission on the target nucleus itself) and the thick target correction were considered. For $\Delta E = 3$ MeV, the overall correction factor is 1.26, the Schwinger term alone being 1.22. The corrected cross section has been checked to be independent of the precise value of ΔE, within a reasonable range. Moreover, for a given ΔE, the correction changes by less than 6% (which means about 1.2% in the corrected cross section) when the proton energy varies within the acceptance of the spectrometer. Hence, an averaged value was used. In the following sections of this paper, we will only consider the corrected data.

3. The experimental (e, e'p) cross section

The use of a liquid deuterium target makes it difficult to extract an absolute cross section. We shall discuss now the various corrections to the raw cross sections, and the results of an absolute measurement on a solid target. The experimental coincidence cross sections are given at the end of this section.

3.1. CORRECTIONS TO THE CROSS SECTIONS

Besides the radiative corrections which have been described above, the raw cross sections must be corrected for the variable target thickness, the electronic dead time and the solid angles of the spectrometers. Beam intensities of 5 to 12 μA were used in this experiment. In this range of currents the target thickness decreases as indicated

by the single arm electron scattering yields, measured at constant angle and momentum for each of the kinematics of table 2. We have used these electron yields to make relative normalizations of the coincidence data. Corrections of the order of 20% were observed depending on the focusing conditions used. These corrections include also the dead time losses in the "600" electronics.

As one moves off the spectrometer axis, the solid angle decreases rapidly. The full aperture length at the target location, normal to the spectrometer axis, is ±2.5 mm in the "900" and ±1.5 mm in the "600". For the 15 mm diameter liquid target and for a laboratory scattering angle of 90°, the ratio of the average solid angle to the one at the target center is 0.87 for the "900" and 0.83 for the "600".

3.2. ABSOLUTE CROSS SECTION

An absolute measurement has been done near $p = 0$ with a deuterated polyethylene target (CD_2, >98% enriched) and a 100 nA beam intensity. The target was measured before and after beam exposure, showing a 6% decrease in mass for the region struck by the beam. A chemical analysis of the hydrogen plus deuterium content of the irradiated part of the target gave 96% of the expected deuterium quantity if pure CD_2. Data have been corrected accordingly.

The missing energy spectrum of this experiment is shown on fig. 8. The small hydrogen contamination gives a rather strong peak, which can be understood if one recalls that the hydrogen momentum distribution is a δ-function.

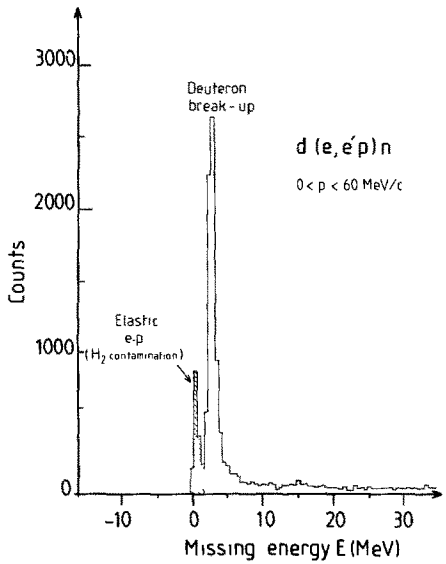

Fig. 8. Missing energy spectrum for the d(e, e'p)n reaction on a solid CD_2 target. The energy bin is 0.25 MeV. The energy resolution of ~0.7 MeV is sufficient to clearly separate the contribution due to the 4% hydrogen contamination in the target (hatched area).

3.3. COINCIDENCE CROSS SECTION

The coincidence cross sections are listed in table 3 and plotted in fig. 9 as a function of the recoil momentum n'. In order to allow an easier comparison with theory, the sixfold differential experimental cross section has been first integrated over the missing energy, then multiplied by the appropriate jacobian to be reduced to the usual fivefold differential cross section $d\sigma/de'd\Omega_{e'}d\Omega_{p'}$. Data for the solid and liquid targets and for the two kinematical conditions are shown. The cross section at 5 MeV/c for the CD_2 target is enhanced by the hydrogen radiative tail (fig. 8) and is omitted in the plot. A comparison of the liquid and solid target cross sections in the range $n' = 15$ MeV/c to $n' = 55$ MeV/c shows a good agreement. However, coincidence elastic electron–proton scattering measurements on a CH_2 target have shown that the whole apparatus underestimates the coincidence cross sections by a factor of 0.83. The corresponding correction has been applied to the data. Moreover, as some changes were made in the apparatus during the time separating the two runs

TABLE 3

Coincidence cross sections $d\sigma/de'd\Omega_{e'}d\Omega_{p'}$ for the CD_2 (two sets of measurements) and liquid deuterium targets as a function of the recoil momentum n', and for the $k = 450$ MeV/c and $k = 350$ MeV/c kinematics

Solid CD_2 target $k = 450$ MeV/c		Liquid target (low n') $k = 450$ MeV/c		Liquid target (high n') $k = 350$ MeV/c	
n' (MeV/c)	cross section (nb · sr^{-2} · MeV^{-1})	n' (MeV/c)	cross section (nb · sr^{-2} · MeV^{-1})	n' (MeV/c)	cross section (nb · sr^{-2} · MeV^{-1})
Set I					
5	112.4±8.3	5	80.3±2.1	155	0.883±0.050
15	73.3±3.8	15	76.9±1.2	165	0.612±0.039
25	55.1±2.8	25	60.6±0.8	175	0.452±0.033
35	37.9±2.5	35	42.5±0.8	185	0.389±0.023
45	23.5±2.4	45	26.9±0.8	195	0.320±0.019
55	14.7±2.3	55	13.73±0.44	205	0.260±0.017
Set II					
5	140.3±13.0	65	9.59±0.22	215	0.195±0.014
15	106.5±6.0	75	6.04±0.18	225	0.172±0.011
25	60.8±4.8	85	4.11±0.13	235	0.113±0.007
35	42.0±4.8	95	2.96±0.11	245	0.123±0.010
45	26.4±7.2	105	1.851±0.095	255	0.095±0.007
		115	1.210±0.040	265	0.072±0.005
		125	0.982±0.019	275	0.063±0.005
		135	0.779±0.019	285	0.050±0.006
		145	0.499±0.026	295	0.037±0.003
		155	0.369±0.024	305	0.025±0.003
		165	0.317±0.013	315	0.028±0.003
		175	0.170±0.012	325	0.022±0.003
				335	0.015±0.003

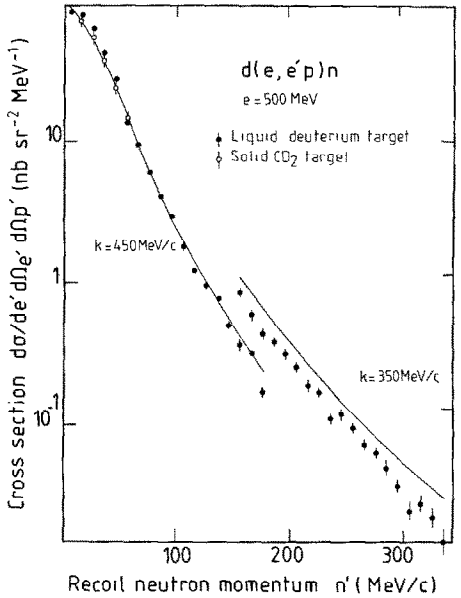

Fig. 9. Coincidence cross section $d\sigma/de'd\Omega_{e'}d\Omega_{p'}$ for the d(e, e'p)n reaction, as a function of the recoil momentum n', for the two sets of kinematical conditions given in table 3. Open circles correspond to measurements on a solid CD_2 target. The solid curve is a PWIA calculation using eq. (1) and a deuteron wave function from the Reid soft core potential, normalized to the low momentum data, as discussed in sect. 5.

– corresponding to the two sets of kinematic conditions – some measurements under kinematics I were repeated during the second run. By comparing the corresponding single arm cross sections, the proton detection system was found to have an efficiency of 0.84 in the second run, thus a 1.20 correction factor was applied to the coincidence cross sections for this run.

In the region of overlap between the two kinematics, one has

$$\sigma/K\sigma_{ep}|_{\text{kinem II}} = (0.90 \pm 0.07)\, \sigma/K\sigma_{ep}|_{\text{kinem I}},$$

where $\sigma/K\sigma_{ep}$ is the coincidence cross section divided by the first two factors of eq. (1). This gives one confidence in the factorization approximation of eq. (1), although it permits a 5 to 10% difference in the absolute response of the apparatus for the two kinematics. Unfortunately, no absolute calibration can be done for the conditions of kinematics II, where $p = 0$ is not allowed.

4. Corrections to the plane wave impulse approximation

In order to extract the deuteron momentum distribution from the (e, e'p) cross section, one has to check the validity of PWIA under the kinematical conditions chosen in the experiment. In this section, we discuss briefly the most important corrections, which are illustrated by the diagrams of fig. 10, that is:

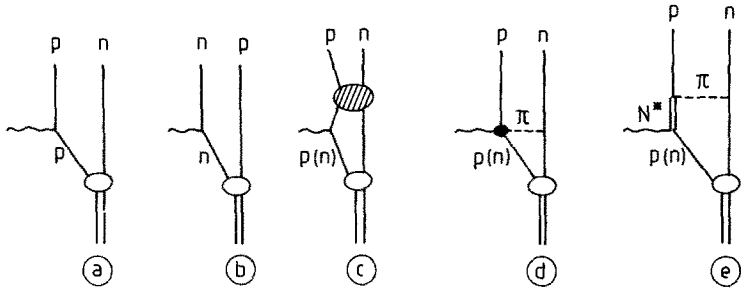

Fig. 10. The most important processes contributing to the d(e, e'p)n cross section at high energy: (a) PWIA e-p scattering, (b) PWIA e-n scattering, (c) final-state interactions, (d) meson exchange pair current, (e) isobar excitation.

(i) The contribution from the electron–neutron quasi-free scattering, with the detection of the spectator proton, and from the interference term between e-p and e-n scattering amplitudes.

(ii) The nucleon off-mass shell effects.

(iii) The n-p final-state interactions.

(iv) The interaction effects in the deuteron ground state, mainly from mesonic exchange currents [17]) and isobar configurations [18]).

4.1. e-n SCATTERING CONTRIBUTION

In order to decide whether the kinematics correspond to quasi-free e-p or e-n conditions, it is more appropriate to consider the n-p c.m. frame of reference. One sees in table 2 that, in each of the two electron kinematic conditions used, the magnitude of the outgoing nucleon momentum in this frame, $p^{\text{c.m.}}$, has been kept constant, the momentum distribution being described by varying its angle $\theta^{\text{c.m.}}$ relative to the direction of the momentum transfer. The conditions for quasi-free scattering on protons (neutrons) are $\theta^{\text{c.m.}} \simeq 0°$ (180°), and $u \simeq M_{\text{p}}^2$ ($t \simeq M_{\text{n}}^2$) where t and u are the usual invariants constructed from the deuteron (d), proton (p_1'), and neutron (p_2') four vectors

$$t = (d - p_1')^2, \qquad u = (d - p_2')^2 . \tag{4}$$

Calculations of the (e, e'p) cross section including the contribution of e-n scattering have been carried out by Durand [19]) and Renard *et al.* [20]) in terms of the different quadratic combinations of the charge and magnetic nucleon form factors $G_{\text{E}}^{\text{n,p}}$ and $G_{\text{M}}^{\text{n,p}}$.

Close to the quasi-free point for the proton ($\theta^{\text{c.m.}} \approx 0°$) Renard *et al.* have shown that the main contributions of the e-n amplitude are through the $G_{\text{M}}^{\text{p}} G_{\text{M}}^{\text{n}}$ interference term in the transverse cross section, and $G_{\text{E}}^{\text{p}} G_{\text{M}}^{\text{n}}$ in the longitudinal one, but that these corrections are of the order of 1%.

However, at the highest values of n' in our kinematics II, $\theta^{\text{c.m.}}$ is as large as 75°, far from both quasi-free points.

We have estimated the e-n scattering contributions in the kinematical conditions corresponding to the highest neutron momentum measured (335 MeV/c). We used formula (II, 4) from ref. [19]), which takes into account the deuteron D-state, and in which we inserted the nucleon form factors using the dipole formula. The contributions from quasi-free e-n scattering, and from the interference term were both found to reduce the (e, e'p) cross section by ~7%. The deuteron wave function was computed from the Holinde–Machleidt [21]) potential, although the result would not be modified qualitatively by the use of any other realistic wave function.

4.2. OFF MASS SHELL EFFECTS

Only kinematical aspects of these effects are taken into account in the expression we used to compute the "half-off shell" e-p scattering amplitude [see appendix of ref. [22])]. Dynamical aspects have been considered by several authors [23,24]). Nyman [24]) gives an expression for the magnetic isoscalar and isovector form factors as a function of the energy distance Δ from the mass shell:

$$\Delta = u^{1/2} - M_{\text{p}} = ((M_{\text{d}} - E'_{\text{n}})^2 - \boldsymbol{n}'^2)^{1/2} - M_{\text{P}} . \tag{5}$$

In our kinematics, the corresponding corrections to the cross section are a few per cent for the largest value of Δ (~120 MeV), so these effects have not been considered in our analysis.

4.3. FINAL-STATE INTERACTIONS

Final n-p state interactions (FSI) can be taken into account by replacing the plane wave of the outgoing proton by a scattering wave calculated from the same potential as for the bound state. Such a calculation has been done by Kingma and Dieperink [25]) who consider FSI only in the $l = 0$ states, taking the higher multipoles from a plane wave. This reduces the cross section by about 10%, essentially above $n' =$ 200 MeV/c. The fact that FSI give rather small contributions in our kinematics is partly due to our choice of quite large values for $E_{\text{np}}^{\text{c.m.}}$. Felder *et al.* [27]), in a systematic study of FSI effects in the d(p, 2p)n reaction, have shown that they are essentially important below $E_{\text{np}}^{\text{c.m.}} \simeq 20$ MeV. However, it was shown by Fabian and Arenhövel [26]) that FSI for the higher multipoles (they consider $l \leqslant 6$) may also contribute significantly, especially at large values of $\theta^{\text{c.m.}}$ (>40°). Their calculation shows that this parameter also is very important when discussing FSI in quasi-free scattering.

4.4. MESON EXCHANGE CURRENTS

Of the various exchange current contributions, the pair current term appears to be the most important, and is the only one included in the calculation of Kingma and

Dieperink [25]). It increases the cross section by ~20% at $n' \sim 300$ MeV/c. A similar and even larger effect is found by Fabian and Arenhövel [26]) who considered π, ρ and ω exchange together with internal degrees of freedom of the nucleon in terms of isobar configurations, which contribute also to the longitudinal part of the cross section. Their calculation shows an enhancement of these effects at relatively small momentum transfer along a line $E_{np}^{c.m.}$ (MeV) $\simeq 60\ k^{c.m.2}$ (fm^{-2}); our kinematics II ($E_{np}^{c.m.} = 121$ MeV, $k^{c.m.2} = 2.77$ fm^{-2}) is not far from this line.

Finally, although we have seen here that, especially at high momenta, several effects may each contribute of the order of 10% to the (e, e'p) cross section, we shall stay in the framework of the PWIA to discuss our results. The reasons are (a) because only partial theoretical estimates are presently at our disposal, indicating effects of the order of our experimental uncertainties, and (b) because only PWIA permits a simple comparison of our data to other experimental results especially with results from (p, 2p) reactions. Thus, the "effective momentum distribution" obtained from the experimental cross section by use of eq. (1) (PWIA) will be directly compared to deuteron wave functions. However, it is clear from the preceding discussion that a more complete calculation would be necessary for a fully quantitative interpretation of the data.

5. The deuteron momentum distribution

5.1. RESULTS OF THE PWIA ANALYSIS

The deuteron momentum distribution has been extracted from our data using the PWIA expression for the coincidence cross section given by eq. (1). Following ref. [22]), and with the notations of fig. 1, the first part of the cross section has been approximated by:

$$K\frac{d\sigma^{(p)}}{d\Omega_{e'}} = \frac{\alpha^2}{q^4}\frac{|\boldsymbol{p}'|e'}{E_p e}\cdot\frac{1}{1-q^2/(M_p+M_p^*)^2}\left\{G_E^2(4p_0p_1'\times p_0'p_1'+q^2M_p^2)\right.$$
$$\left.-\frac{q^2}{(M_p+M_p^*)^2}G_M^2(2(p_0p_1')^2+2(p_0'p_1')^2-q^2M_p^2)\right\}, \qquad (6)$$

where $M_p^* = \sqrt{p_1^2} \neq M_p$ is the initial "bound proton" mass defined by energy and momentum conservation. The proton electric and magnetic form factors G_E and G_M have been calculated on the mass shell according to Janssens *et al.* [28]).

Due to the energy and angular acceptances of the apparatus, different sets of the kinematical parameters lead to the same magnitude for the neutron recoil momentum $\boldsymbol{n}'$ (or initial proton momentum $\boldsymbol{p}$). This has been properly taken into account by computing $K(d\sigma^{(p)}/d\Omega_{e'})$ for each kinematical configuration feeding a given p-momentum bin, and weighting the events accordingly.

The momentum distribution is listed in table 4 up to 340 MeV/c in 10 MeV/c momentum bins, and plotted in fig. 11. Around 160 MeV/c an average of the values

TABLE 4

The effective deuteron momentum distribution extracted from the d(e, e'p)n cross section of table 3. Data from both targets and both kinematics are included

p (MeV/c)	$\rho(p)$ (MeV/c)$^{-3}$	p (MeV/c)	$\rho(p)$ (MeV/c)$^{-3}$
5	$0.1209 \pm 0.003 \times 10^{-5}$	175	$0.200 \pm 0.015 \times 10^{-8}$
15	$0.1133 \pm 0.0017 \times 10^{-5}$	185	$0.162 \pm 0.009 \times 10^{-8}$
25	$0.875 \pm 0.012 \times 10^{-6}$	195	$0.126 \pm 0.007 \times 10^{-8}$
35	$0.604 \pm 0.011 \times 10^{-6}$	205	$0.986 \pm 0.062 \times 10^{-9}$
45	$0.375 \pm 0.011 \times 10^{-6}$	215	$0.712 \pm 0.052 \times 10^{-9}$
55	$0.188 \pm 0.006 \times 10^{-6}$	225	$0.612 \pm 0.039 \times 10^{-9}$
65	$0.129 \pm 0.003 \times 10^{-6}$	235	$0.393 \pm 0.028 \times 10^{-9}$
75	$0.800 \pm 0.024 \times 10^{-7}$	245	$0.416 \pm 0.033 \times 10^{-9}$
85	$0.535 \pm 0.017 \times 10^{-7}$	255	$0.317 \pm 0.024 \times 10^{-9}$
95	$0.380 \pm 0.014 \times 10^{-7}$	265	$0.238 \pm 0.016 \times 10^{-9}$
105	$0.234 \pm 0.012 \times 10^{-7}$	275	$0.206 \pm 0.014 \times 10^{-9}$
115	$0.151 \pm 0.005 \times 10^{-7}$	285	$0.162 \pm 0.017 \times 10^{-9}$
125	$0.121 \pm 0.003 \times 10^{-7}$	295	$0.121 \pm 0.010 \times 10^{-9}$
135	$0.949 \pm 0.023 \times 10^{-8}$	305	$0.080 \pm 0.009 \times 10^{-9}$
145	$0.601 \pm 0.032 \times 10^{-8}$	315	$0.090 \pm 0.008 \times 10^{-9}$
155	$0.424 \pm 0.025 \times 10^{-8}$	325	$0.072 \pm 0.008 \times 10^{-9}$
165	$0.327 \pm 0.017 \times 10^{-8}$	335	$0.048 \pm 0.008 \times 10^{-9}$

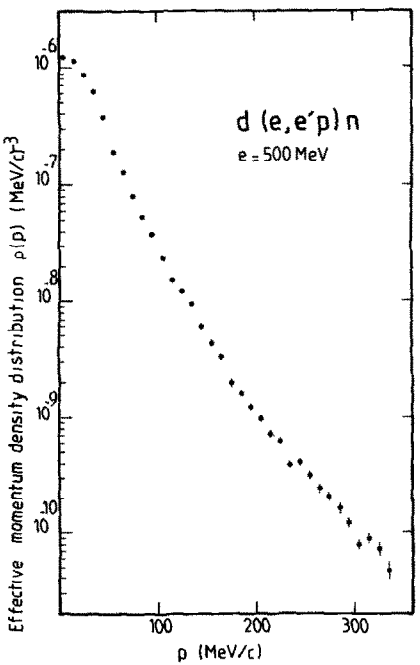

Fig. 11. The momentum distribution in the deuteron from the d(e, e'p)n reaction at 500 MeV.

of the two kinematics has been considered. As mentioned in sect. 3, one sees no noticeable discontinuity in the distribution in this region. The values coming from the measurements on solid CD_2 targets have also been included in the tabulated distribution.

5.2. COMPARISON WITH PREVIOUS EXPERIMENTAL RESULTS

The existing data on the deuteron momentum distribution coming from quasi free scattering experiments are summarised in table 5. No other (e, e'p) data are presently available. For the (p, 2p) or (p, pn) results, we have only considered experiments performed at sufficiently high energy that the impulse approximation is essentially valid, and in which the momentum density was scanned within a sufficiently wide range.

TABLE 5

Quasi-free scattering measurements of the nucleon momentum distribution of the deuteron

Reaction	Lab.	Incident energy (MeV)	p_{max} (MeV/c)	Ref.
(p, 2p)	SREL	600	370	Perdrisat *et al.* [29])
(p, 2p)	SREL	585	425	Witten *et al.* [30])
(p, 2p)(p, pn)	LAMPF	800	350	Felder *et al.* [31])
	SREL	585	350	
(e, e'p)	Orsay	350	95	Bounin [11])
(e, e'p)	Kharkov	1195	185	Antoufiev *et al.* [12])
		1180	300	Agranovich *et al.* [13])
(e, e'p)	Saclay	500	340	present experiment

These results present the common feature of a pronounced enhancement of the momentum distribution above $p \simeq 200$ MeV/c relative to the theoretical predictions. This is illustrated in fig. 12, where for the sake of clarity, the experimental results are normalized to a model deuteron density, i.e. the Hulthén S-state plus 7% Yamaguchi D-state wave function given in ref. [30]). This wave function has been generally used in the analysis of the previous experiments. One sees clearly that our results deviate strongly from the others above $p \simeq 180$ MeV/c, even by an order of magnitude around 300 MeV/c.

With regard to the (p, 2p) experiments, it has been thought [30,32]) that this excess of cross section may arise from final-state interactions. In fact, the kinematics in the SREL/LAMPF experiments are such that the relative n-p center of mass energy in the final unbound system is small, of a few tens of MeV, even decreasing at large initial proton momenta [30]). However, as is shown, for example, in the analysis of Wallace [32]) for the results from Perdrisat *et al.* [29]), FSI do not give a sufficiently high contribution to explain the theory-experiment divergence at high momenta.

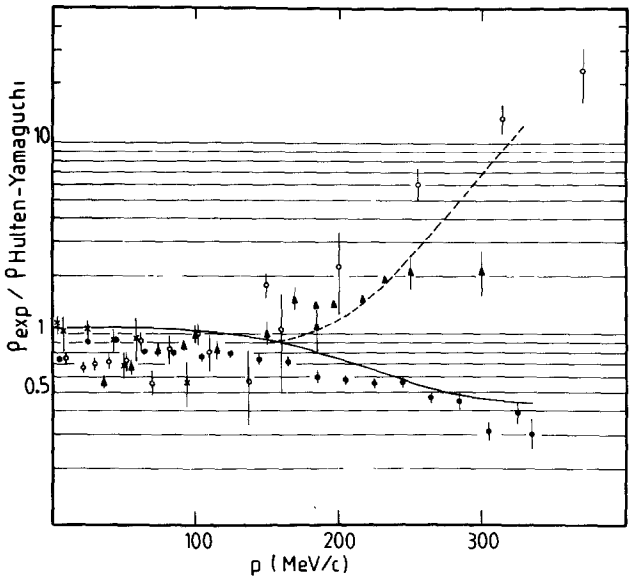

Fig. 12. Ratio of the experimental momentum distribution to the Hulthén–Yamaguchi momentum distribution in (p, 2p) and (e, e'p) reactions. Data are ○ (p, 2p) Perdrisat *et al.* [29]); × (e, e'p) Bounin [11]); ▲ (e, e'p) Agranovich *et al.* [13]); ● (e, e'p) Saclay, present experiment. The dashed curve is a smooth interpolation through the data points of Felder *et al.* [31]), in the (p, 2p) reaction at 800 MeV, 40°+40°. The full line is the ratio of the Holinde–Machleidt momentum distribution (HM2) to the Hulthén–Yamaguchi one.

Concerning the (e, e'p) results from Kharkov, it is even more unlikely that FSI could explain the observed discrepancy which starts at around $p = 160$ MeV/c, since $E_{np}^{c.m.}$ is too large (about 160 MeV) to make FSI an important contribution.

Moreover, as in our experiment, the energy transfer is below or close to the coherent pion production threshold, so this process cannot contribute for such a proportion.

In the low momentum region, the experimental results are located below the theoretical curve. It is interesting to compare the normalisation factor f that one must apply to the Hulthén density to fit the various sets of data. This is done in table 6, for $0 < p < 200$ MeV/c. Although differences exist from one experiment to another concerning the exact meaning of the quoted uncertainties – most being purely statistical – one sees that f is close to 0.85 for all the experiments except the one from Bounin [11]), and the (p, pn) experiment from Felder *et al.* [31]). This last value is still questionable, and might be due, according to the authors, to a large neutron background in the experiment. A recent experiment by James *et al.* [34]) gives $f_{p,pn}/f_{p,2p} = 1.08 \pm 0.08$, instead of the value 1.47 ± 0.16 in the Felder experiment. With regard to our data, we estimate the non-corrected systematic errors such as the extrapolation to a null beam current of the effective target density to be no larger than 7%.

TABLE 6

Ratio, f, of experimental to theoretical (Hulthén) momentum densities from deuteron break-up in the momentum range $0 < p < 200$ MeV/c.

Reaction	f	Ref.
(p, 2p)	0.84 ± 0.04	Perdrisat *et al.* [29])
	0.87	Witten *et al.* [30])
	0.89 ± 0.04	Felder *et al.* [31])
(p, pn)	1.31 ± 0.13	Felder *et al.* [31])
(e, e'p)	0.99 ± 0.05	Bounin [11])
(e, e'p)	0.85 ± 0.01	Antoufiev [12])
(e, e'p)	0.82 ± 0.02	present experiment

5.3. COMPARISON WITH THEORETICAL DEUTERON WAVE FUNCTIONS

In the preceding section, a Hulthén wave function was used as a guide to compare various experimental deuteron momentum distributions. However, it is clear from fig. 12 that, even if one normalises the theoretical curve by 0.82 to fit the low momentum part of the distribution, such a wave function is not able to reproduce our data at high momenta. In this section, we compare our results to those obtained from three other wave functions computed from more realistic nucleon–nucleon potentials: the Reid soft core (RSC) potential [35]), the "Paris" potential [36]) of Vinh Mau *et al.* (VM), and the "Bonn" one-boson exchange potential [21]) of Holinde and Machleidt in the so called HM2 version. The predictions of these potentials for the deuteron ground-state properties are summarised in table 7, together with the most recent experimental values for the deuteron D-state asymptotic normalization and quadrupole moment.

Fig. 13 shows the corresponding momentum distributions in comparison with our data. To fit the low momentum region, the theoretical curves have been multiplied by: 0.82 for RSC, 0.84 for VM and 0.81 for HM2. The Hulthén–Yamaguchi (HY) wave function is also shown, normalised by a factor of 0.82. One sees clearly that

TABLE 7

Deuteron ground-state properties from various nucleon–nucleon potentials (P_D: deuteron D-state percentage, ρ_D: asymptotic normalisation, Q: quadrupole moment); the most recent experimental values of ρ_D and Q are also quoted

NN potential	P_D	ρ_D	Q	Ref.
Reid soft core	6.47	0.028	0.280	[35])
Paris	5.46	0.026	0.277	[36])
Holinde–Machleidt 2	4.32	0.026	0.287	[21])
experimental values		0.0263 ± 0.0013	0.2875 ± 0.002	[37,8])

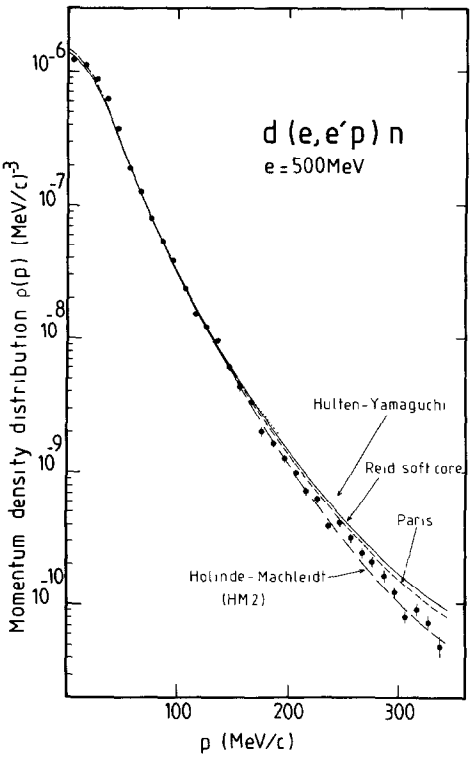

Fig. 13. The experimental "effective nucleon momentum distribution" of the deuteron compared to various theoretical calculations. Each theoretical curve has been normalised to give the best fit to the data in the range $0 < p < 200$ MeV/c. The normalisation factors are 0.82 for the Hulthén–Yamaguchi distribution (dotted line), 0.82 for Reid soft core (full line), 0.84 for Paris (dashed line) and 0.81 for Holinde–Machleidt distribution (dot-dashed line).

more realistic wave functions are in much better agreement with the data. The experimental uncertainties do not permit one to distinguish between the RSC and VM potentials, which give very similar distributions in this momentum range. The best fit is obtained in using the Holinde–Machleidt potential, which leads to the smallest D-state percentage, as shown in table 7. However a definite statement concerning the best choice of any of these wave functions cannot be done without a complete calculation of the (e, e'p) cross section which includes the contributions of the other processes mentioned in sect. 4.

6. Conclusion

The very simple reaction mechanism assumed for the d(e, e'p)n reaction in fig. 1 appears to be essentially valid for the kinematic conditions chosen in this experiment. Accordingly, the (e, e'p) reaction at high energy provides a clean tool to determine

the deuteron momentum density. With the duty factor of the Saclay linac, it was possible to extend the previous (e, e'p) data up to $p = 340$ MeV/c, in a region where the D-state contribution dominates the density. In this region, a strong difference with previous (e, e'p) and (p, 2p) experiments is observed, a difference which can be accounted for only partially by invoking final-state interaction effects in the (p, 2p) case.

As in most of the previous experiments, the experimental cross section is ~15% lower than the PWIA prediction in the low momentum region, this value being quite independent of the ground-state deuteron model used. However to make a precise determination of this deviation is still a challenge.

Although the accuracy of the data is sufficient to clearly discern between Hulthèn-type and more realistic deuteron wave functions, one needs to go to higher p (~500 MeV/c) to fully explore the D-state region. To do so, one has to be able to measure cross sections 4 to 5 times smaller. With regard to the last point $p =$ 335 MeV/c, for which the true over accidental coincidences ratio is still 0.7 in the 3 MeV missing energy bin considered, it is likely that this can be achieved with slight improvements of the apparatus, such as a better time resolution. An increase in the incident energy would also be very helpful.

On the other hand, the interpretation of the high-momentum part of the density is much more complex, as effects like mesonic exchange currents, isobars contributions, . . . , may here dominate. In fact these effects are precisely those that give rise to the D-state itself [38]), and only a complete calculation treating them on the same footing as the D-state nuclear configurations would make sense in interpreting the high momentum region. In sect. 4, we ignored relativistic effects in the ground-state wave function (like P-state contributions), since they have been shown to be significant only at much larger momenta [39]).

We are indebted to C. Tzara and Ph. Catillon for their interest and encouragement in this experiment, and to F. Netter and the ALS staff for the high quality of the beam. We wish to thank A. Godin and his group for providing us with the liquid deuterium target. The close collaboration of E. Auriol, L. Cohen, J. Dupont, J. Le Dévéhat, M. Lefèvre, G. Lemarchand and J. Millaud, in operating the detection and acquisition systems, made the experiment possible. We acknowledge very fruitful discussions and correspondence with Ingo Sick, H. Arenhövel, A.E.L. Dieperink, G.G. Simon, R. Vinh Mau and H. Zingl.

References

1) M. Gourdin, Diffusion des électrons de haute énergie (Masson, Paris, 1966)
2) R. Budnitz *et al.*, Phys. Rev. **173** (1968) 1357
3) W. Bartel *et al.*, Phys. Lett. **30B** (1969) 285

4) G.G. Simon *et al.*, Phys. Rev. Lett. **37** (1976) 739;
G.G. Simon *et al.*, Nucl. Phys. **A324** (1979) 277;
D. Royer *et al.*, Contribution to Int. Conf. on nuclear physics with electromagnetic interactions, Mainz, June 5–9, 1979
5) G. Jacob and T.A.J. Maris, Nucl. Phys. **32** (1962) 169
6) R.J. Adler, Phys. Rev. **141** (1966) 1499
7) D. Royer, Proc. Workshop on few body systems and electromagnetic interactions, Frascati, 1978; Lecture Notes in Physics **86** (1978) 172
8) R.V. Reid and M.L. Vaida, Phys. Rev. Lett. **29** (1972) 494
9) R.D. Amado *et al.*, Phys. Lett. **79B** (1978) 368;
R.E. White *et al.*, Nucl. Phys. **A321** (1979) 1
10) M. Croissiaux, Phys. Rev. **127** (1962) 613
11) P. Bounin, Ann. de Phys. **10** (1965) 475
12) Y.P. Antoufiev *et al.*, ZhETF Pisna **19** (1974) 657 [JETP Lett. **19** (1974) 339];
Y.P. Antoufiev, Yad. Phys. **22** (1975) 236 [Sov. J. Nucl. Phys. **22** (1976) 121]
13) U.L. Agranovich, V.S. Kuzmenko and P.V. Sorokin, Yad. Phys. **25** (1977) 1123
14) P. Leconte *et al.*, Nucl. Instr. **169** (1980) 401
15) A. Godin *et al.*, Prog. Rep. of the Nucl. Phys. Dept., CEA note N-2070, Saclay, 1979
16) L.W. Mo and Y.S. Tsai, Rev. Mod. Phys. **41** (1969) 200
17) M. Chemtob and M. Rho, Nucl. Phys. **A163** (1971) 1
18) A.M. Green, Rep. Progr. Phys. **39** (1976) 1109;
H.J. Weber and H. Arenhövel, Phys. Reports **36C** (1978) 277
19) L. Durand III, Phys. Rev. **115** (1959) 1020
20) F.M. Renard *et al.*, Nuovo Cim. **38** (1965) 565
21) K. Holinde and R. Machleidt, Nucl. Phys. **A256** (1976) 479
22) J. Mougey *et al.*, Nucl. Phys. **A262** (1976) 461
23) A.M. Bincer, Phys. Rev. **118** (1960) 855
24) E.M. Nyman, Nucl. Phys. **A154** (1970) 97
25) G. Kingma and A.E.L. Dieperink, Phys. Lett. **78B** (1978) 375
26) W. Fabian and H. Arenhövel, Nucl. Phys. **A314** (1979) 253
27) R.D. Felder *et al.*, Nucl. Phys. **A280** (1977) 308
28) T. Janssens *et al.*, Phys. Rev. **142** (1966) 922
29) C.F. Perdrisat *et al.*, Phys. Rev. **187** (1969) 1201
30) T.R. Witten *et al.*, Nucl. Phys. **A254** (1975) 269
31) R.D. Felder *et al.*, Nucl. Phys. **A264** (1976) 397
32) J.M. Wallace, Phys. Rev. **C5** (1972) 609
33) B.M. Golovin *et al.* Sov. J. Nucl. Phys. **16** (1973) 602
34) A.N. James *et al.*, Nucl. Phys. **A324** (1979) 253
35) R.V. Reid, Ann. of Phys. **50** (1968) 411
36) M. Lacombe *et al.*, Phys. Rev. **D12** (1975) 1495; **C21** (1980) 861
37) H.E. Conzett *et al.*, Phys. Rev. Lett. **43** (1979) 572
38) M. Rho, Proc. Intermediate Energy Summer School, Erice, Sicily 1976
39) W.W. Buck and F. Gross, Phys. Rev. **D20** (1979) 2361